Journal of Power Sources 273 (2015) 966–980

Contents lists available at ScienceDirect

Journal of Power Sources

journal homepage: www.elsevier.com/locate/jpowsour

A techno-economic analysis and optimization of Li-ion batteries for light-duty passenger vehicle electrification

Apurba Sakti [a], Jeremy J. Michalek [b, c, *], Erica R.H. Fuchs [b], Jay F. Whitacre [b, d]

[a] Department of Chemical Engineering, and The Energy Initiative, Massachusetts Institute of Technology, Cambridge, MA 02139, USA
[b] Department of Engineering and Public Policy, Carnegie Mellon University, Pittsburgh, PA 15213, USA
[c] Department of Mechanical Engineering, Carnegie Mellon University, Pittsburgh, PA 15213, USA
[d] Department of Materials Science and Engineering, Carnegie Mellon University, Pittsburgh, PA 15213, USA

HIGHLIGHTS

- We analyze EV Li-ion NMC-G battery & pack designs and optimize for minimum cost.
- Economies of scale are reached quickly at ~200–300 MWh annual production.
- Small-pack PHEV applications use high power cells with thinner electrodes (base case \$545 kWh^{-1}).
- Large-pack BEV applications use lower cost cells with thicker electrodes (base case \$230 kWh^{-1}).
- Increased electrode thickness capabilities could reduce BEV pack cost by an additional 8%.

ARTICLE INFO

Article history:
Received 5 June 2014
Received in revised form
9 September 2014
Accepted 10 September 2014
Available online 22 September 2014

Keywords:
Electric vehicle
Lithium-ion battery
Battery design
Production cost
Electrode thickness

ABSTRACT

We conduct a techno-economic analysis of Li-ion NMC-G prismatic pouch battery and pack designs for electric vehicle applications. We develop models of power capability and manufacturing operations to identify the minimum cost cell and pack designs for a variety of plug-in hybrid electric vehicle (PHEV) and battery electric vehicle (BEV) requirements. We find that economies of scale in battery manufacturing are reached quickly at a production volume of ~200–300 MWh annually. Increased volume does little to reduce unit costs, except potentially indirectly through factors such as experience, learning, and innovation. We also find that vehicle applications with larger energy requirements are able to utilize cheaper cells due in part to the use of thicker electrodes. The effect on cost can be substantial. In our base case, we estimate pack-level battery production costs of ~\$545 kWh^{-1} for a PHEV with a 10 mile (16 km) all-electric range ($PHEV_{10}$) and ~\$230 kWh^{-1} for a BEV with a 200 mile (320 km) all-electric range (BEV_{200}). This 58% reduction, from \$545 kWh^{-1} to \$230 kWh^{-1}, is a larger effect than the uncertainty represented by our optimistic and pessimistic scenarios. Electrodes thicker than about 100 or 125 microns are not currently used in practice due to manufacturing and durability concerns, but relaxing this constraint could further lower the cost of larger capacity BEV_{200} packs by up to an additional 8%.

1. Introduction

In 2012, the United States consumed about 366 million gallons of gasoline per day, accounting for 66% of US transportation energy and 47% of US petroleum consumption [1]. Electrified vehicles (EVs), including PHEVs, which use a mix of petroleum and electricity, and BEVs, which use only grid electricity, offer the potential to greatly reduce US gasoline consumption [2]. When electricity is generated from clean sources, electrified vehicles can also contribute to reducing greenhouse gas (GHG) emissions and air pollution damages [3,4].

The cost of Li-ion batteries is arguably the single largest barrier to mainstream adoption of EVs [5–7]. Thus, battery cost is a key factor in addressing oil dependency, global warming, and air pollution in the United States. We investigate the role of battery design variables on the cost and performance of Li-ion batteries by

* Corresponding author. Department of Engineering and Public Policy, Carnegie Mellon University, Pittsburgh, PA 15213, USA. Tel.: +1 412 268 3765.
E-mail address: jmichalek@cmu.edu (J.J. Michalek).

http://dx.doi.org/10.1016/j.jpowsour.2014.09.078
0378-7753/

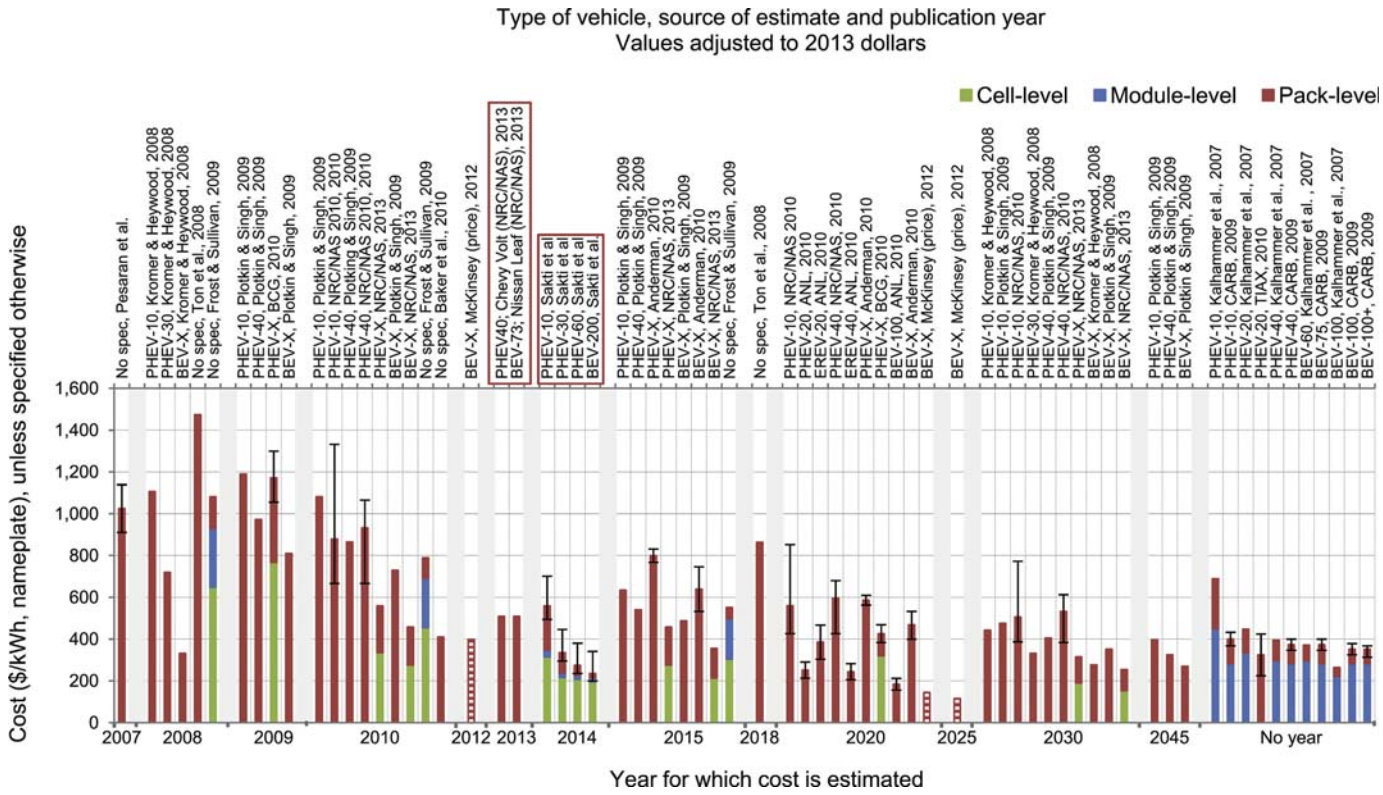

Fig. 1. Summary of available cost estimates of lithium-ion batteries for different vehicular applications. Vehicle all-electric-range (AER) shown in miles. The costs were assumed to be at the pack-level for the nameplate capacity unless otherwise specified in the reports. Wherever ranges were specified, error bars have been used to show the upper and the lower bounds. For reports with ranges, if the most probable cost estimate was not specified, the average of the lower and the upper cost estimate is shown as the base estimate. In the case of McKinsey, the estimates are for the price, which includes profit margins. Price estimates are shown using the red and white striped columns to avoid confusion with cost estimates. Battery cost estimates for the Chevy Volt (PHEV35) and a Nissan Leaf (BEV75), in 2012, has also been shown [7,15–28]. All cost estimates have been adjusted to 2013 dollars using GDP deflators for the US [29]. (For interpretation of the references to color in this figure legend, the reader is referred to the web version of this article.)

Table 1
Summary of key assumptions/considerations in Li-ion battery cost studies. Vehicle all-electric-range (AER) shown in miles.

Study	Key assumptions/considerations
NRC/NAS, 2013 [15]	Assumes costs for Chevy Volt and Nissan Leaf are \$500 kWh^{-1}, future costs are projected based on historical cost pattern for 18650 cells. 18650 cells declined by more than 95% in 20 years. Midrange BEV pack cost assumed to decline by 45%. PHEV pack costs assumed to be \$60–70 kWh^{-1} higher than BEV packs.
McKinsey, July 2012 [16]	Prices in 2011 dollars per effective kWh. Uses a 70% depth-of-discharge. Three major contributors to decrease in prices by 2025: manufacturing at scale, lower component prices, and battery capacity-boosting technologies. Plot shows McKinsey's price estimate scaled to dollars per nameplate kWh.
Boston Consulting Group, 2010 [17]	15 kWh NCA pack. The 2009 cost structure include a complete pack-level bill of materials, direct and indirect plant labor, equipment depreciation, R&D, scrap rates, and overhead markup. Costs estimated at a production volume of 50,000 cells or 500 battery packs in 2009 and 73 million cells or 1.1 million packs in 2020. Based on BCG analysis, information from Argonne National Laboratory, and interviews with component manufacturers, cell producers, tier one suppliers, OEMs, and academic experts.
NRC/NAS, 2010 [18]	Report includes three cost ranges for probable, conservative and an optimistic case for $PHEV_{10}$ and $PHEV_{40}$ batteries. Report considers a 4 kWh battery pack for a $PHEV_{10}$ and a 16 kWh battery pack for a $PHEV_{40}$.
TIAX, 2010 [19]	Estimates for a $PHEV_{20}$. 5.5 kWh of useable energy. Packs designed for capacities of 6.9–9.8 kWh to account for 30% capacity fade. Report studies 5 chemistries: NCA, NCM, LFP, LMO, LL-NMC. Prismatic (wound) cells.
ANL, 2010 [20]	Four chemistries reported: LMO-G, NMC-G, LFP-G, NCA-G. PHEV20: 62 kW (10 s), 10.3 kWh packs. $EREV_{20}$: 148 kW (10 s), 9.6 kWh packs. $EREV_{40}$: 158 kW (10 s), 18.7 kWh packs. BEV_{100}: 154 kW (10 s), 33.3 kWh packs.
Baker et al., 2010 [21]	Expert elicitation. 10 year funding trajectories considered. With \$150 M yr^{-1} funding, there is a 66% chance of the cost being less than \$200 yr^{-1} and a 20% chance of it being less than \$90 kWh^{-1}. \$384 kWh^{-1} was the base value mentioned on one instance.
Anderman, ARB Feedback, 2010 [22]	Feedback to CARB cost estimate. Gives ranges for EV battery costs at 500 MWh in 2015 and at 2500 MWh in the 2018–2020) timeframe. Cost of PHEV batteries per nominal kWh greater than EV batteries by 20–30%.
Plotkin and Singh, 2009 [7]	Factory gate prices for $PHEV_{10}$, $PHEV_{40}$, and BEV_{100} batteries in 2008\$. Costs based on literature and include optimistic and 'still more optimistic' outlook based on DOE goals. Literature includes: Kromer and Heywood (2007), EPRI (2005), Kalhammer (2007), and Anderman (email comm., 2008)
California ARB, 2009 [23]	Cost ranges at module and pack level provided for batteries for a $PHEV_{10}$, $PHEV_{40}$/BEV_{75}, BEV_{100}, and a BEV_{100+}. Upper bound is for an APV of 500 MWh and the lower bound for 2500 MWh. Battery pack sizes-$PHEV_{10}$: ~7 kWh, $PHEV_{40}$/BEV_{75}: ~16 kWh, BEV: 24+ kWh. Numbers updated since Kalhammer (2007) using $PHEV_{20}$ pack size from TIAX (2009) and the same scaling factors as Kalhammer (2007).
Frost and Sullivan, 2009 [24]	Based on interviews with 12 companies: battery manufacturers and OEMs. Reports cost. However, states that prices will drop by 20–70% when cell production rises from 1 million per annum to reach more than 50 million per annum.
Kromer and Heywood, 2008 [25]	Uses the formula: Battery Cost = (Cost_High Energy) × f(Power-to-Energy Ratio). Current costs based on cost multipliers from Ford Motor Company, a base cost of \$300 kWh^{-1} base cost, and assumes improvements in energy density etc. Assumes decrease in material costs for high-energy battery at a rate of 2.5% per year for 20 years. Future high-energy battery cost estimated to be \$250 kWh^{-1} and \$200 kWh^{-1} in the optimistic case. Present-day high-power lithium-ion batteries incur a factor of 4.5–5 cost penalty compared to high-energy batteries. Future high-power battery uses a factor of 3 for the cost penalty.
Ton et al., 2008 (Sandia) [26]	Capital cost, no further description provided. Results of a literature review and discussions with technology leaders at national laboratories and in industry
Kalhammer et al., 2007 (California ARB) [27]	Based on estimates from three different manufacturers at production rates of 500 MWh and 2500 MWh using 45 Ah cells, and numbers from ANL (Nelson). Uses scaling factors to convert data into module-level specific costs. The following pack capacities were used: Full BEV: 40 kWh (120 Ah cells), Small BEV: 25 kWh (45 Ah cells), $PHEV_{40}$: 14 kWh (45 Ah cells), $PHEV_{20}$: 7 kWh (25 Ah cells), $PHEV_{10}$: 4 kWh (12 Ah cells)
Pesaran et al., 2007 (NREL) [28]	High-energy Li-ion batteries, no further specification.

first characterizing the tradeoffs in battery design and subsequently using this knowledge to optimize and assess technical and economic implications.

Existing studies on the economics, adoption potential, and emissions reduction potential of EVs typically treat Li-ion batteries as though they are all the same, with a single estimate of cost per kWh of storage [3,5,8–12]. In practice, Li-ion technology encompasses a wide range of alternative chemistries (e.g.: $LiMn_2O_4$, $LiFePO_4$, $LiNi_{0.33}Mn_{0.33}Co_{0.33}$, etc.), electrode designs (e.g.: thin/thick), packaging alternatives (prismatic, pouch, cylindrical), and capacities (size, number of electrode layers, etc.) of the individual cells that make up the pack as well as differences in pack configuration, thermal management, and control electronics. Each of the potential combinations of these alternatives has different performance, cost, weight, volumetric, thermal, and degradation characteristics that interact with the constraints and needs in the design of a vehicle powertrain system. For example, short-range PHEVs require cells with higher power-to-energy ratios because they have less battery capacity over which to distribute peak power demands. Thinner electrodes deliver higher power per unit capacity, but they also require more of the inactive materials, and this has implications for cost, volume, weight, and life [13,14].

Fig. 1 summarizes existing public EV Li-ion battery cost estimates separated into cell, module, and pack level costs wherever available, and Table 1 summarizes key assumptions and considerations from the relevant studies. Fig. 1 also includes results from this study, which are discussed later. Estimates reveal (1) an expected decrease in cost over time, (2) generally lower costs per kWh for higher capacity packs (e.g.: BEV vs. PHEV), and (3) substantial variation in cost estimates from different sources. We aim to produce a transparent, bottom–up assessment that explicitly accounts for the battery design changes needed to meet requirements for various EV applications at minimum cost while identifying key factors and characterizing uncertainty.

2. Approach

We construct an optimization model to identify the least-cost battery and pack design that satisfies energy and power requirements representative of $PHEV_{10}$ (16 km AER), $PHEV_{30}$ (48 km AER), $PHEV_{60}$ (96 km AER), and BEV_{200} (320 km AER) vehicles, where the subscript indicates the vehicle's all-electric range (AER) in miles. We first introduce the form of the model and then develop detailed models for battery performance and cost.

2.1. Formulation

We aim to solve the following optimization problem:

Minimize $C(\mathbf{x})$	Minimize battery pack cost
With respect to $\mathbf{x} = [x_W, x_T, x_L, x_N, x_M]^T$	With respect to the cell's width, electrode thickness, and number of bi-cell layers and the number of cells per module and number of modules per pack
Subject to $P(\mathbf{x}) \geq P^{PEAK}$ $E(\mathbf{x}) \geq E^{AER}$ $c^{MIN} \leq c(\mathbf{x}) \leq c^{MAX}$ $\mathbf{x}^{MIN} \leq \mathbf{x} \leq \mathbf{x}^{MAX}$ $x_T, x_W \in \mathbb{R}$ $x_L, x_N, x_M \in \mathbb{Z}$	Subject to: - The pack's power capabilities must satisfy the vehicle's peak power requirements - The pack's energy capacity must satisfy vehicle energy requirements - Each cell must have a capacity within bounds - All decision variables must be within their respective bounds - Cathode width and thickness are continuous, and the number of layers, cells per module, and modules per pack are integers.

Table 2
Parameter values used for optimization. Vehicle all-electric-range (AER) shown in miles. Power and energy requirements based on [30].

		$PHEV_{10}$	$PHEV_{30}$	$PHEV_{60}$	BEV_{200}
E^{AER}	Energy requirement (kWh)	3.6	8	16.5	48
P^{PEAK}	Power requirement (kW)	48.6	44	47.9	80
c^{MIN}	Minimum cell capacity	10 Ah			
c^{MAX}	Maximum cell capacity	60 Ah			
$\mathbf{x}^{MIN}$	Lower variable bounds	[50 mm, 25 μm,5,5,4]^T			
$\mathbf{x}^{MAX}$	Upper variable bounds	[150 mm, 125 μm, 200,50,22]^T			

where x_W is the cathode width (mm), x_T is the cathode thickness (μm), x_L is number of bi-cell layers in each cell, x_N is the number of cells per module, x_M is the number of modules per pack, and the functions $C(\mathbf{x})$, $P(\mathbf{x})$, $E(\mathbf{x})$, and $c(\mathbf{x})$ are defined later in this section. Parameter values for energy and power requirements are summarized in Table 2 for each vehicle type, based on [30]. Fig. 2 shows a schematic of the cathode width, the cathode thickness and the number of bi-cell layers in a cell. The cells in a module, and the modules in a pack are all connected in series, similar to the design outlined in ANL's BatPaC [31]. Table 2 also lists the simple bounds used for each variable as well as bounds on cell capacity. These bounds are intended only as practical constraints for modeling tractability, and they are generally inactive at solutions (we highlight exceptions in results).

2.2. Battery performance model

To compute cell capacity for an arbitrary design, we compute the volume of active material (where each bi-cell layer contains twice the cathode thickness), multiply by the density and the specific capacity of the active material, and divide by 10^9 to express the result in Ah. The resulting formula for cell capacity is:

$$c(\mathbf{x}) = \frac{2x_T x_L a x_W^2 s m \rho}{10^9} \quad (1)$$

where a is the cell's assumed aspect ratio ($a = 3$), s is the specific capacity of the cathode active material (150 mAh g^{-1}), m is the mass fraction of the active material in the cathode (89%), and ρ is the cathode density (2.546 g m^{-3}).

To compute pack energy, we multiply pack capacity by average cell voltage:

$$E(\mathbf{x}) = V_{NMC}^{AVG} x_N x_M c(\mathbf{x}) \quad (2)$$

where $V_{NMC}^{AVG} = 3.73$ for NMC333 cells, estimated using Battery Design Studio™ (BDS) simulation software.

To compute pack power capabilities, we conduct simulation experiments using BDS, which was previously validated for this application using laboratory tests with physical cells [32]. BDS was used to simulate the hybrid pulse power characterization (HPPC) test on a set of 48 virtual $LiNi_{0.33}Mn_{0.33}Co_{0.33}$/Graphite (NMC333-G) cells varied over a full factorial of selected electrode thickness and cell capacity levels. In particular, the single side electrode coating thickness was varied from 25 μm to 200 μm in intervals of 25 μm and the cell capacity was varied from 10 Ah up to 60 Ah in 10 Ah intervals. The HPPC test procedure, defined by the United States Advanced Battery Consortium (USABC), is used to test the dynamic power capability of a battery pack and consists of both discharge and charging current pulses [33]. The HPPC test result gives the 10-s discharge-pulse and regen-pulse power capability of the battery-pack at 10% depth-of-discharge (DoD) increments [33]. The goal

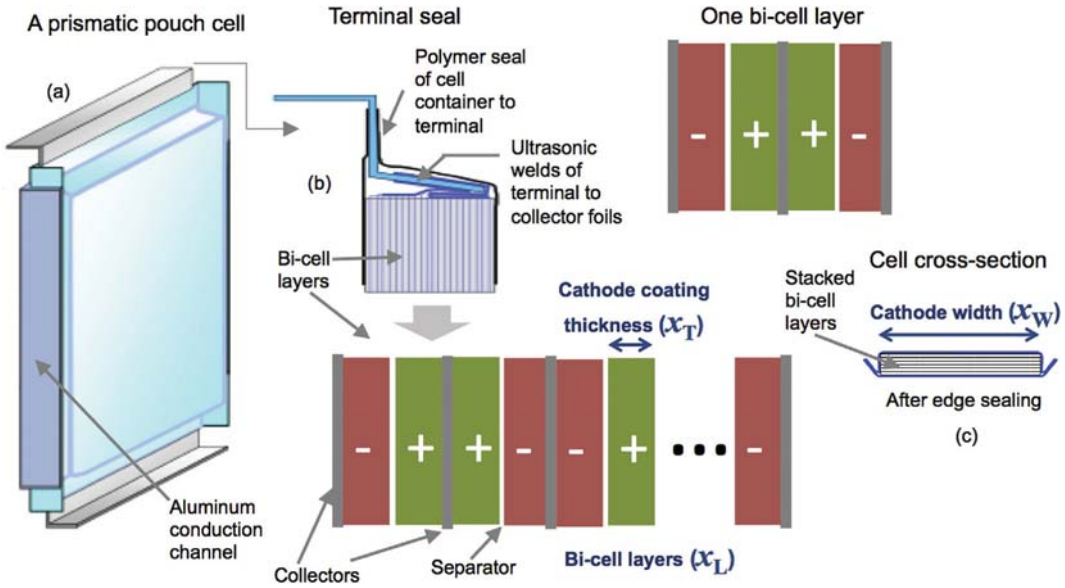

Fig. 2. Illustration of the following three decision variables: cathode width, cathode coating thickness, and the number of bi-cell layers. Pictures (a), (b), and (c) have been adapted from ANL's BatPaC model documentation, with permission from ANL [31].

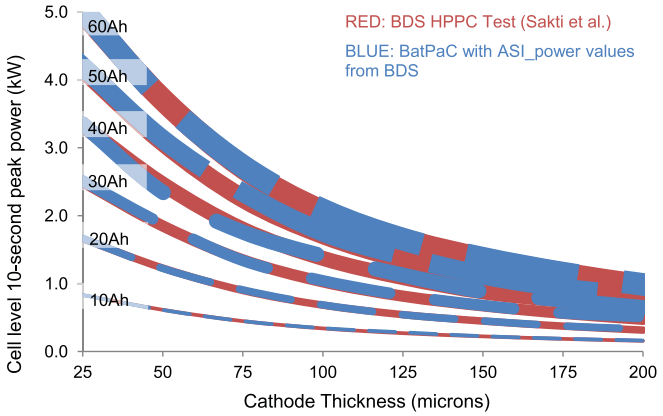

Fig. 3. Comparison of the 10-s power values calculated using 1) the power meta-model developed by Sakti et al. using BDS (Equation (3) and 2) BatPaC, using the ASI values from BDS. The results are seen to match up well.

with this test is to determine the pulse power capability of a battery pack at the minimum allowable state of charge (SoC) value.

See Supplementary information for the 10-s power capabilities of the 48 cell designs. Using Eureqa Formulize [34] to identify a suitable function form for regression, the following relationship was established:

$$P(\mathbf{x}) = x_N x_M \left(\frac{x_T c(\mathbf{x})}{\beta_1 + \beta_2 x_T^{\beta_3} - x^T} - \beta_4 x_T c(\mathbf{x}) \right) \quad (3)$$

where the constants, identified through regression, are $\beta_1 = 149$, $\beta_2 = 0.281$, $\beta_3 = 2$, $\beta_4 = 8.98 \times 10^{-6}$. Residuals between the 10-s power performance values from BDS and those predicted from the regression model fall within a maximum error of 0.03 kW which is between 0.02 and 0.04% of the peak power requirements for the applications considered in this study. Note that this model assumes all cells are arranged in series. Different series/parallel arrangements are left for future work but are not expected to substantially change cost-minimizing design implications.

As a reality check, the area-specific impedance (ASI) values calculated for the 48 different cell designs were used as inputs to compute the 10-sec power capability using the equations listed in ANL's BatPaC [31]. The ASI values are similar to those reported elsewhere by BatPaC authors [35]. Fig. 3 shows the comparison of the 10-s power results from BDS and those from the equations used in BatPaC, where thicker lines are used to indicate larger capacity cells. Results are similar, indicating confidence in the use of our regression model.

2.3. Battery pack production cost

To compute cost $C(\mathbf{x})$, we model the process of manufacturing the Li-ion battery pack. Li-ion battery manufacturing involves multiple process steps, summarized in Fig. 4. We implement a process-based cost model (PBCM) to simulate production operations in a manufacturing plant, using data at the individual machine level for each of the process steps. Inputs such as machine and installation cost, equipment processing rate, fractional use of labor, process step yield, batch size, cycle time, unplanned downtime, etc. are specified for each process step. The inputs and decision rules (e.g. equations) for the variables making up each process step are generally expressed as functions of design decisions.

Technical cost modeling was developed to explore the economic implications of new technologies (e.g. Refs. [36,37]) and to estimate production costs during early stages of product development (e.g. Refs. [38,39]). PBCM is a pioneer of these costing methods, and we follow the approach here (Refs. [40–43]).

We adopt information on equipment cost and processing rates for most of the process steps from Argonne National Laboratory's Li-ion battery cost and performance model, BatPaC [31]. BatPaC is the only other bottom–up cost model currently available in the public literature that estimates the performance and cost of a battery design [31]. Material requirements to build a Li-ion battery pack of a given design were also calculated using the equations listed in BatPaC [31].

BatPaC models economies of scale by first estimating costs (equipment, labor, etc.) for a base case of 100,000 battery packs per

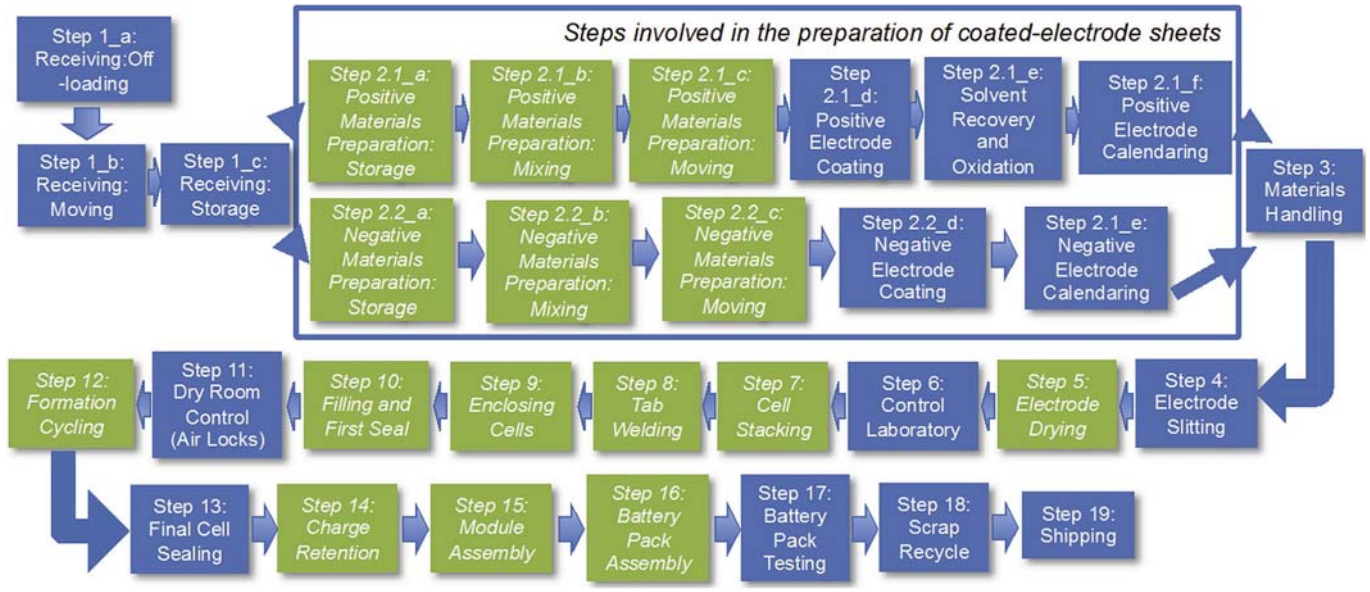

Fig. 4. Process steps involved in Li-ion battery manufacturing (adopted from ANL's BatPaC [31]). Process steps with sufficient data on machine processing rates are assumed to be dedicated, and have been shown in green boxes with italicized fonts. Blue boxes show the process steps for which sufficient information was not available, and they were therefore considered undedicated. (For interpretation of the references to color in this figure legend, the reader is referred to the web version of this article.)

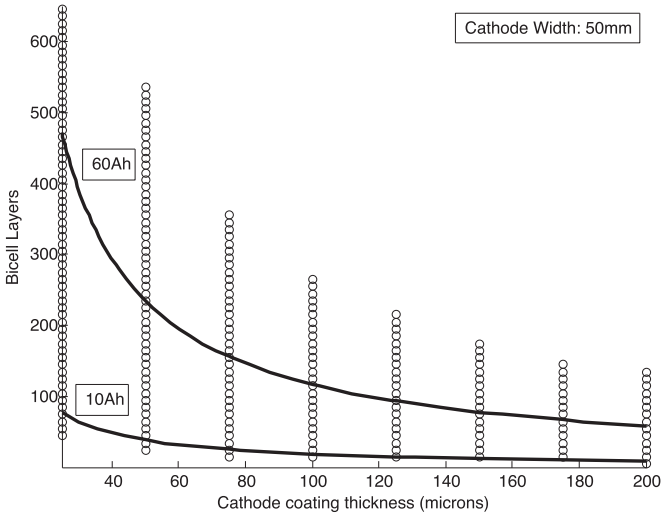

Fig. 5. An example of the design grid for cells of 50 mm cathode width. The solid lines show the region of interest between cell capacities of 10 Ah–60 Ah.

year and then scaling these estimates exponentially to estimate costs at other production volumes: $c_\alpha = c_\alpha^O(R_\alpha/R_\alpha^O)^{p_\alpha}$, where c_α^O is the unit cost (or usage value) of production cost type α (equipment, labor, material, space, etc.) for the baseline processing rate R_α^O associated with the baseline production volume of 100,000 packs per year; c_α is the unit cost (or usage value) associated with the new processing rate R_α; and p_α is the power factor used to scale the cost for that production cost type. Values used for p_α in BatPaC are generally around 0.4–0.5 for labor and relatively higher at 0.6–0.8 for plant floor-space and the cost of capital equipment.

The advantage of this approach is that it is simple and requires less information to construct a model. The disadvantages are that the lower-unit-cost equipment needs for producing at higher volume are treated as a black box without identifying whether such equipment could be developed or what the respective prices and process variable changes (such as cycle times, yields and scrap rates) would be. Although versatile and fairly comprehensive, BatPaC neglects the discrete equipment investments (and associated technical developments) needed to realize changes in production volume, and it ignores differences in yield rates at different process steps and for different design. Finally, BatPaC ignores the

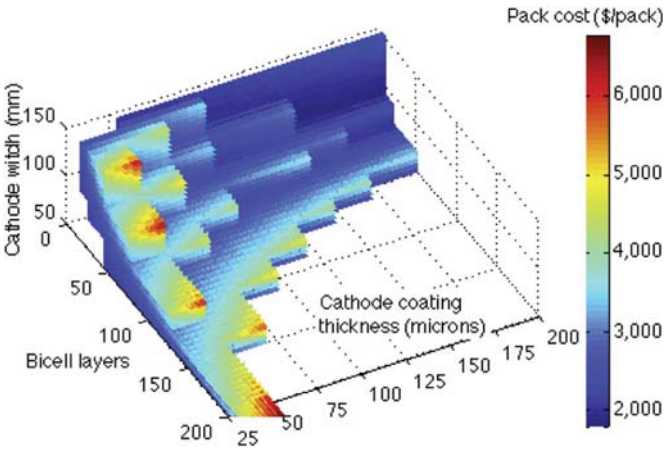

Fig. 6. Pack cost ($ pack^{-1}) as a function of cathode thickness, cathode width, and number of bi-cell layers for 10 cells per module and 4 modules per pack evaluated at points in the design grid that surround and include cell capacities from 10 to 60 Ah.

time value of money in building and equipment investment. Building on BatPaC's data and foundation, we address each of these limitations in our model.

A PBCM uses process-step-level data to estimate the resource requirements, including capital, labor, materials and energy, to meet production targets for a given design. Each process step may produce both acceptable and unacceptable units, so steps earlier in the process must produce additional units in order to generate sufficient acceptable units at the final step. The requirement for each element is calculated taking into account the yield of each process step, which is incorporated using the following formula for the effective production volume.

$$v_{i-1} = \frac{v_i}{y_i(\mathbf{x})} \quad \forall i \in \{1, 2, \ldots, n\} \tag{4}$$

where v_i is the annual effective production volume output at step i, v_{i-1} is the input volume required at step i, y_i is the yield rate at step i, and v_n is the specified final annual production volume output following the final step n [42]. When yield rates vary with the design choices $\mathbf{x}$, the effective production volume $v_i \quad \forall i \in \{1, 2, \ldots, n-1\}$ at each process step is also a function of $\mathbf{x}$. The yield rate assumptions are given in Table 3 for our base case and in Table 6 and Fig. 7 for our sensitivity cases. Given a specified final production volume output v_n, Eq. (4) is used recursively to determine the effective volume needed at each prior process step. The unit cost $C(\mathbf{x})$ of producing this output is the sum of the total annual costs incurred over each process step divided by the final production volume:

Table 3
Facility-wide and design-related base case model assumptions.

Input	Base	Units
Facility wide operating parameters		
Working days yr^{-1} (t^{DPY})	300	days yr^{-1}
No shifts (t^{NS})	0	h day^{-1}
Unpaid breaks (t^{UB})	2	h day^{-1}
Paid breaks (t^{PB})	1	h day^{-1}
Building space (p^{BLD})	3000	$ m^{-2}
Direct wage, with benefits (p^{LBR})	18	$ h^{-1}
Discount rate (r)	10	%
Lifetime for cost elements (l_{ij})		
Capital recovery period ($j \in J_i^{EQP}$)	6	yrs
Building recovery period ($j \in J_i^{BLD}$)	20	yrs
Facility wide additional costs		
Auxiliary equipment (γ^{AUX})	10	% of main machine cost
Maintenance (γ^{MNT})	10	% of main machine cost
Fixed overhead (γ^{OH})	35	% of other fixed costs
Energy cost (γ^{ERG})	3	% of material and labor costs
Design-related process assumptions		
Cell-level		
Cell cathode chemistry	NMC333-G	–
Aspect ratio of each electrode (a)	3	–
Mass fraction of the active material in the cathode	0.89	–
Mass fraction of the active material in the anode	0.95	–
Production volume (v_n)	20,000	packs yr^{-1}
Yield rate (y_i)		
Cell stacking step ($i = 7$)	95	%
All other steps ($i \neq 7$)	100	%
Scrap rates		
Positive electrode material (dry) (step#2.1a)	7.8	%
Negative electrode material (dry) (step#2.2a)	7.8	%
Positive current collector (Al) (step#2.1d)	9.8	%
Negative current collector (Cu) (step#2.2d)	9.8	%
Separators (step#7)	2	%

Table 4
Equipment assumptions for each process step based on information from BatPaC [31].

Step#	Step name	Equipment cost with installation (p_{ij}^{EQP}) ($)	Footprint (θ_i) (m^2)	Fractional use of labor (L_i)	Processing rate $(t_i^{CYC})^{-1}$	Unplanned downtime (t_i^{UD})	Dedicated?	Notes/comments
1a	Receiving: off-loading	600,000	300	1	6667 kg shift^{-1}	20%	No	
1b	Receiving: moving	1,200,000	300	1	6667 kg shift^{-1}	20%	No	
1c	Receiving: storage	1,800,000	300	1	6667 kg shift^{-1}	20%	No	
2.1a	Positive materials preparation: storage	1,000,000	200	1	1000 lit shift^{-1}	25%	Yes	
2.1b	Positive materials preparation: mixing	500,000	200	1	1000 lit shift^{-1}	25%	Yes	
2.1c	Positive materials preparation: moving	500,000	200	0.67	1000 lit shift^{-1}	25%	Yes	
2.1d	Positive electrode coating	9,500,000	750	4	10 m min^{-1}	30%	No	Width of coater: 1.5 m, Solvent evaporation rate: 11.2 s kg^{-1}, solvent evaporation ovens: $1,200,000
2.1e	Solvent recovery and oxidation	3,000,000	225	2	212 kg h^{-1}	20%	No	
2.1f	Positive electrode calendaring	1,000,000	225	2	10 m min^{-1}	30%	No	Calendaring width: 1.5 m, assumed to match the coater
2.2a	Negative materials preparation: storage	1,000,000	200	0.67	900 lit shift^{-1}	25%	Yes	
2.2b	Negative materials preparation: mixing	500,000	200	0.67	900 lit shift^{-1}	25%	Yes	
2.2c	Negative materials preparation: moving	500,000	200	0.67	900 lit shift^{-1}	25%	Yes	
2.2d	Negative electrode coating	9,500,000	750	4	10 m min^{-1}	30%	No	Solvent evaporation rate: 17 s kg^{-1}, width of the coater: 1.5 m, solvent evaporation ovens: $1,200,000
2.2e	Negative electrode calendaring	1,000,000	225	1	10 m min^{-1}	30%	No	Calendaring width: 1.5 m, assumed to match the coater
3	Materials handling	1,500,000	900	4	1135 m^2 h^{-1}	20%	No	
4	Electrode slitting	2,000,000	300	4	1135 m^2 h^{-1}	20%	No	
5	Electrode drying	200,000	38	0.25	600 kg shift^{-1}	20%	Yes	
6	Control laboratory	1,500,000	300	4	121 kWh h^{-1}	20%	No	
7	Cell stacking	1,000,000	150	1.25	225 bicell-layers min^{-1}	20%	Yes	
8	Tab welding	1,000,000	150	1.25	5 cells min^{-1}	20%	Yes	
9	Enclosing cells	750,000	150	0.75	5 cells min^{-1}	20%	Yes	
10	Filling and first seal	1,250,000	225	1.25	5 cells min^{-1}	20%	Yes	
11	Dry room control (air locks)	20,000,000	100	2	0.03 m^2 m^{-2} dry room area	–	No	
12	Formation cycling	857,143	63	0.23	See notes	20%	Yes	Batch size: 500 cells cycler^{-1}, cycle time: 57,600 s
13	Final cell sealing	2,000,000	450	2	15 cells min^{-1}	20%	No	
14	Charge retention	6333	1.2	0.004	See notes	20%	Yes	Batch size: 500 cells, cycle time: 1,209,600 s
15	Module assembly	1,500,000	150	1.5	280 cells h^{-1}	20%	Yes	
16	Battery pack assembly	1,000,000	150	1	See notes	20%	Yes	Processing rate: 6 packs h^{-1} with 4 modules pack^{-1}
17	Battery pack testing	3,000,000	450	3	14 packs h^{-1}	20%	No	
18	Scrap recycle	2,500,000	600	5	441 kg shift^{-1}	20%	No	
19	Shipping	5,000,000	900	6	121 kWh h^{-1}	5%	No	

$$C(\mathbf{x}) = \frac{C^{MTL} + C^{EQP} + C^{BLD} + C^{LBR} + C^{ERG} + C^{AUX} + C^{MNT} + C^{OH}}{v_n} \quad (5)$$

where C^{MTL}, C^{EQP}, C^{BLD}, C^{LBR}, C^{ERG}, C^{AUX}, C^{MNT} and C^{OH} are the annual material, equipment, labor, building, energy, auxiliary equipment, maintenance, and overhead costs, respectively. Each cost element is potentially a function of the design **x**. Material cost C^{MTL} was calculated using BatPaC equations [31]. For other costs, it is necessary to compute the number of machines or laborers needed at each process step to achieve the target volume v_n of battery packs per year. For process steps where we have sufficient data on available line time per discrete unit of equipment, we assume these steps to be dedicated to the production of the product being analyzed, and we compute the minimum number of machines (integer) needed to produce the required volume of products from that process step [43]. For other process steps, because we lack the required information to compute integer requirements, we treat the steps as non-dedicated and compute the fractional number of machines needed to manufacture the required annual production volume. This has the potential effect of smoothing the cost-vs.-production-volume curve and may introduce some error. For instance, in the case of the *dedicated* process step #2.1a, named "positive materials preparation: storage", when effective production volume at that step exceeds the capacity of a single machine, a second machine is purchased, causing a discontinuity in the unit-cost vs. production–volume curve. In contrast, for non-dedicated process step #4, named "electrode slitting", a fractional number of machines is permitted, resulting in a continuous unit-cost vs.

Table 5
Design decision variable values considered for the design grid.

Variable	Description	Domain	Resolution	Units
x_T	Single side cathode coating thickness	[25, 200]	25	μm
x_L	Number of bicell-layers each cell	[5, 645[a]]	10	–
x_W	Width of the cathode	[50, 250]	25	mm
x_N	Number of cells in a module	[5, 50]	5	–
x_M	Number of modules in a pack	[4, 22]	2	–

[a] Data were not collected for all combinations of values but only enough to enable interpolation between 10 and 60 Ah (see Fig. 5 for an example).

Table 6
Process-based cost model parameters and their values for the sensitivity analysis.

		Base	Optimistic	Pessimistic	Notes
Process parameters	Working days yr^{-1}	300	360	240	Base: ANL BatPaC. Lower bound: assumed. Upper bound: Brodd 2010 [45].
	Direct wage (w/benefits) ($\$ h^{-1}$)	18	15	25	Upper and lower bounds: Brodd 2010 [45], for skilled/unskilled labor. Base: ANL BatPaC.
	Price of building space ($\$ m^{-2}$)	3000	1600	4000	Base: ANL BatPaC. Lower and upper bounds: assumed.
	Discount rate	10%	6%	14%	Assumed.
	Positive electrode active material price ($\$ kg^{-1}$)	31	31	53	ANL BatPaC.
	Negative electrode active material price ($\$ kg^{-1}$)	19	17	23	ANL BatPaC.
	Separator price ($\$ m^{-2}$)	2	1	2.9	ANL BatPaC.
	Electrolyte price ($\$ liter^{-1}$)	21.6	18	24.5	ANL BatPaC.
	Scrap rate (%)	Table 4	−25%	+25%	Base: ANL BatPaC.
	Yield rate, cell stacking step ($i = 7$) (%)	95%	99%	90%	Base: ANL BatPaC.
Design constraints	Cathode coating thickness	125 microns	200 microns	100 microns	Based on expert opinion.
	10 s EV-x power constraint (kW)	Base	−25%	Base	Base: Kromer and Heywood, 2007 [30]. Lower bound addresses future improvements that may result in lower power requirements like body light-weighting etc.
	EV-x energy constraint (kWh)	Base	−25%	Base	Base: Kromer and Heywood, 2007 [30]. The −25% reflects the future improvement in the mileage obtained from batteries.

production–volume curve. The discontinuities observed in the cost-vs.-production-volume curves shown in Fig. 8 result from the *dedicated* process steps. In general, the number of machines or laborers is computed as:

$$N_{ij}(\mathbf{x}) = \begin{cases} \left\lceil \dfrac{t_i^{CYC} v_i(\mathbf{x})}{t^{DPY}\left(24 - t^{NS} - t^{UB} - t^{PB} - t_i^{UD}\right)} \right\rceil & \forall i \in S_D, j \in J_i^{EQP} \\ \dfrac{t_i^{CYC} v_i(\mathbf{x})}{t^{DPY}\left(24 - t^{NS} - t^{UB} - t^{PB} - t_i^{UD}\right)} & \forall i \in S_{ND}, j \in J_i^{EQP} \\ \dfrac{t_i^{CYC} v_i(\mathbf{x})}{t^{DPY}\left(24 - t^{NS} - t^{UB} - t^{PB} - t_i^{UD}\right)} L_i & \forall i \in S, j \in J_i^{LBR} \end{cases} \quad (6)$$

where S_D is the set of steps that are dedicated, S_{ND} is the set of steps that are non-dedicated, S is the set of all process steps that include both dedicated and non-dedicated, J_i^{EQP} is the set of equipment cost elements in step i, J_i^{LBR} is the set of labor cost elements in step i, t^{DPY} is the number of working days per year (Table 3), t^{NS} is the number of hours with no shifts per day (Table 3), t^{UB} is the number of unpaid hours in breaks per day (Table 3), t^{PB} is the number of paid hours in breaks per day (Table 3), t_i^{UD} is the average hours of unplanned downtime per day for step i (Table 4), t_i^{CYC} is the cycle time (time to produce one unit) for process step i (Table 5),[1] and L_i is the fractional use of labor in step i (i.e.: the fraction of the machine's cycle time for which a laborer must be present). Process steps that are treated as dedicated are shown in Fig. 4 in green boxes (italic fonts), while the process steps treated as non-dedicated are shown in blue boxes.

For annual equipment costs.

$$C^{EQP}(\mathbf{x}) = \sum_{i=1}^{n} \sum_{j \in J_i^{EQP}} \phi_{ij} p_{ij}^{EQP} N_{ij}(\mathbf{x}), \quad (7)$$

where $\phi_{ij} = r(1+r)^{l_{ij}}/((1+r)^{l_{ij}} - 1)$ is the capital recovery factor [42], r is the discount rate (Table 3), l_{ij} is the lifetime of cost element j in step i (Table 3), and p_{ij}^{EQP} is the total (single period) price paid per unit of production equipment (Table 4). For annual building costs

$$C^{BLD}(\mathbf{x}) = \sum_{i=1}^{n} \sum_{k \in J_i^{EQP}} \phi_{ij} p^{BLD} \theta_{ik} N_{ik}(\mathbf{x}), \quad (8)$$

where θ_{ik} is the footprint of equipment k in step i (Table 4) and p^{BLD} is the total (single period) price paid for building space per square foot (Table 3). For annual labor costs

$$C^{LBR}(\mathbf{x}) = \sum_{i=1}^{n} \sum_{j \in J_i^{LBR}} \left(24 - t^{NS} - t^{UB}\right) t^{DPY} p^{LBR} N_{ij}(\mathbf{x}), \quad (9)$$

where p^{LBR} is the hourly labor wage (Table 3). Annual energy costs, auxiliary equipment costs, maintenance costs, and overhead costs are estimated as percentages of other costs:

$$\begin{aligned} C^{ERG}(\mathbf{x}) &= \gamma^{ERG}\left(C^{MTL} + C^{LBR}\right) \\ C^{AUX}(\mathbf{x}) &= \gamma^{AUX} C^{EQP} \\ C^{MNT}(\mathbf{x}) &= \gamma^{MNT} C^{EQP} \\ C^{OH}(\mathbf{x}) &= \gamma^{OH}\left(C^{BLD} + C^{EQP} + C^{AUX} + C^{MNT}\right), \end{aligned} \quad (10)$$

where γ^{ERG} is energy cost as a percent of material and labor cost, γ^{AUX} is auxiliary equipment cost as a percentage of equipment cost, γ^{MNT} is maintenance cost as a percentage of equipment cost, and γ^{OH} is overhead cost as a percentage of building cost, equipment cost, auxiliary equipment cost, and maintenance cost (Table 3).

Facility-wide and design-related base case model assumptions are summarized in Table 3. We assume a yield of 100% for all process steps except Cell Stacking (step #7), where defects may be incorporated as the bi-cell layers are stacked on top of one another. Our base assumption for cell stacking yield is 95%. We examine other cell stacking yield values in sensitivity analyses, including one case where yield rates are dependent on cell design. We assume the aspect ratio of the cathode to be three, following the value used in BatPaC. Mass-fractions in the cathode and the anode of the active material are common values used in the industry. For the base case, a target final annual production volume of v_n = 20,000 battery

[1] In general, cycle time may also be a function of the design, but we ignore the effect of design on cycle time here.

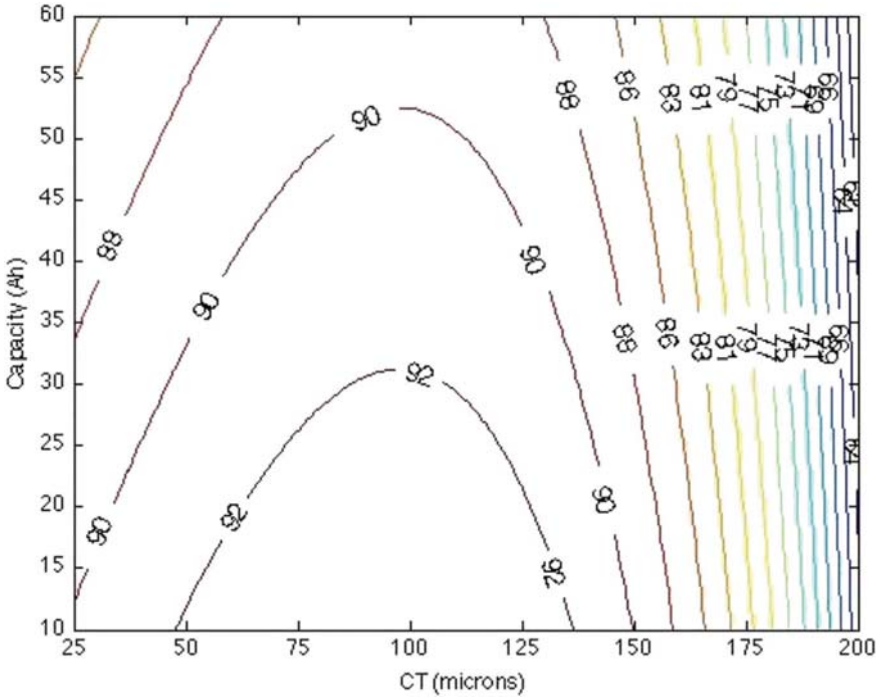

Fig. 7. Overall cell-level yield used in sensitivity scenario as a function of the cathode coating thickness (CT) and cell capacity.

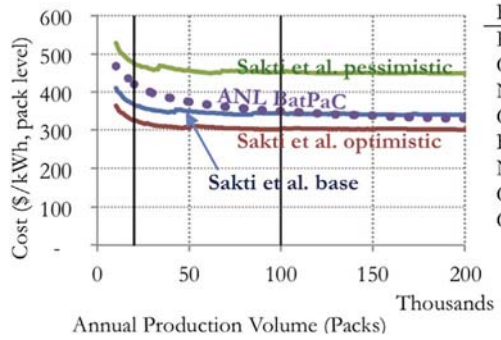

Battery Pack Design Specification	
Energy (kWh)	6.8
Chemistry	NMC333-G
Number of modules	6
Cathode Width (mm)	92
Bi-cell layers	21
Number of cells per module	6
Capacity of each cell (Ah)	50.8
Coating Thicknesses	
Cathode (μm)	140
Anode (μm)	133

Fig. 8. Comparison of BatPaC vs. our PBCM with base case, optimistic, and pessimistic assumptions. Vertical lines show BatPaC's base volume of 100,000 packs and Sakti et al.'s base case of 20,000 packs.

packs was assumed to reflect the upper limit a manufacturer may encounter given present day EV sales. Table 4 lists key assumptions for individual process steps.

While it is possible to use the equations for $C(\mathbf{x})$ directly in optimization, we instead evaluate $C(\mathbf{x})$ over a grid of values for $\mathbf{x}$ and use linear interpolation to estimate the cost of intermediate designs. Table 5 summarizes the grid of points in $\mathbf{x}$ used to sample $C(\mathbf{x})$. For each combination of cathode thickness, cathode width, cells per module, and modules per pack we sample a range of values for number of bi-cell layers using a range large enough to exceed the span from 10 Ah to 60 Ah capacity sufficiently to enable interpolation within that range. By examining only enough points to enable interpolation within the feasible domain, we avoid combinations of design variables that are unreasonable or fall outside of model capabilities, and we reduce computational burden. Interpolation was infeasible at 2 modules per pack, and hence the range of 4–22 packs is reported in Table 5. Fig. 5 shows an example of points evaluated for a 55 mm cathode width, and Fig. 6 shows cost as a function of cathode thickness, cathode width, and the number of bi-cell layers for the set of points evaluated.

2.4. Optimization

Having defined the functions $C(\mathbf{x})$, $P(\mathbf{x})$, $E(\mathbf{x})$, and $c(\mathbf{x})$, the resulting optimization problem can be written as

$$\begin{aligned}
&\text{Minimize } C(\mathbf{x})\\
&\text{With respect to } \mathbf{x} = [x_W, x_T, x_L, x_N, x_M]^T\\
&\text{Subject to } P^{PEAK} - x_N x_M \left(\frac{x_T c(\mathbf{x})}{\beta_1 + \beta_2 x_T^{\beta_3} - x^T} - \beta_4 x_T c(\mathbf{x}) \right) \le 0\\
&\qquad E^{AER} - V_{NMC}^{AVG} x_N x_M c(\mathbf{x}) \le 0\\
&\qquad c^{MIN} \le c(\mathbf{x}) \le c^{MAX}\\
&\qquad \mathbf{x}^{MIN} \le \mathbf{x} \le \mathbf{x}^{MAX}\\
&\qquad x_T, x_W \in \mathbb{R}\\
&\qquad x_L, x_N, x_M \in \mathbb{Z}\\
&\text{where } c(\mathbf{x}) = \frac{2 x_T x_L r x_W^2 s m \rho}{10^9}
\end{aligned}$$

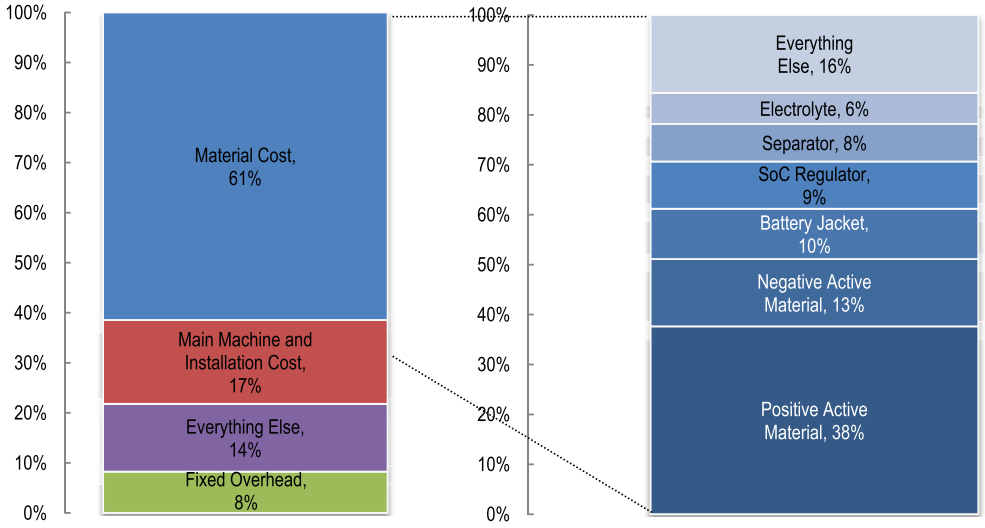

Fig. 9. Total breakdown of the sample $PHEV_{20}$ (36 km AER) battery pack at 20,000 packs per year. Breakdown of the material cost has also been shown.

and where $C(\mathbf{x})$ is a piecewise linear function treated as a black box function. The result is a non-convex mixed-integer nonlinear program (MINLP). We apply BNB20 [44], a branch and bound algorithm, using randomized multistart to search for global minima in our optimization problem. In the base case, out of 10 runs we identified 1 distinct local minima, giving confidence that the best local minimum we identified is likely the global minimum. In addition, we solved a separate problem where the three integer variables were relaxed to the continuous domain to identify a lower bound. This lower bound is similar to the optimal mixed integer solution, with an objective value within 0.5%, providing additional confidence that our solution is globally optimal.

2.5. Sensitivity analysis

The robustness of results was tested using sensitivity analysis. Table 6 lists base case, optimistic, and pessimistic assumptions for each parameter varied in the PBCM and in the design constraints. The power constraint and energy constraint were varied by −25% to account for future developments like vehicle light-weighting, etc. Based on information from battery manufacturing experts, the base case for the maximum allowable cathode coating thickness was assumed to be 125 microns, with an optimistic value of 200 microns and a pessimistic value of 100 microns.

We also investigate a fourth scenario where yield rates vary as a function of cathode thickness and cell capacity. Fig. 7 shows our assumed yield rate map for this case, based on discussion with an industry expert and the following observations: (1) current battery manufacturers are able to produce coatings up to about 125 microns successfully (with a sweet spot of 75–100 microns), but thicker electrodes generate defects in structural integrity and from cracks during drying; (2) cathode layers that are too thin are also difficult to manufacture; and (3) all else being equal, larger capacity cells are more prone to yield loss because more bi-cell layers must be stacked and wired. Our assumed yield equation for this case (obtained using Eureqa) is:

$$y = \beta_1 + \beta_2 x_T - \frac{\beta_3}{\beta_4 - x_T} - \beta_5 c(\mathbf{x}) \tag{11}$$

where the constants, identified through regression, are $\beta_1 = 107.9$, $\beta_2 = 0.183$, $\beta_3 = 5192.8$, $\beta_4 = 266.1$, and $\beta_5 = 0.099$.

3. Results and discussion

We first summarize results from our cost model and then show results for minimum cost battery and pack designs.

3.1. Battery and pack production cost

Fig. 8 compares the cost of a battery and pack design sized for a $PHEV_{20}$ (32 km AER) using BatPaC vs. our PBCM with base case, optimistic, and pessimistic assumptions (Table 6).[2] Results from the base case PBCM are comparable to BatPaC at a volume of 100,000 packs, where BatPaC is calibrated. The PBCM results are lower cost than BatPaC estimates at low production volume and comparable cost at higher volume, since we account explicitly for the effects of economies of scale on line requirements rather than using an assumed exponential relationship. Results from the PBCM suggest that economies of scale are reached at about 200–300 MWh of battery capacity production – much sooner than suggested by the BatPaC model. This early attainment of economies of scale is observed across a wide range of battery pack specifications.

Fig. 9 shows the cost breakdown for the base case cost at 20,000 units per year. Material cost is the single largest cost contributor, accounting for 61% of pack-level costs. Half of material cost stems from the cost of electrode active material. Labor (included with "Everything Else") accounts for less than 5% of total pack-level costs, suggesting that regional variation in labor costs is not a key driver of pack costs.

Fig. 10 summarizes variation in pack-level cost resulting from variation in process parameters and material costs defined in Table 7. For the process step parameters, dry room control processing rate has the largest influence on cost, but a 25% change in processing rate affects pack level cost by less than \$5 kWh^{-1}. This minimal effect on cost leads us to believe that although we did not have more fine-tuned data on potential variations in processing rates, additional efforts to reduce any uncertainty around these variables would not significantly change outcomes. Variation in material cost, on the other hand, has a larger influence on pack cost,

[2] This reference battery and pack design meets requirements for a $PHEV_{20}$ for the Urban Dynamometer Driving Schedule (UDDS) in Powertrain Systems Analysis Toolkit (PSAT) simulations (personal communication with Orkun Karabasoglu, MIT).

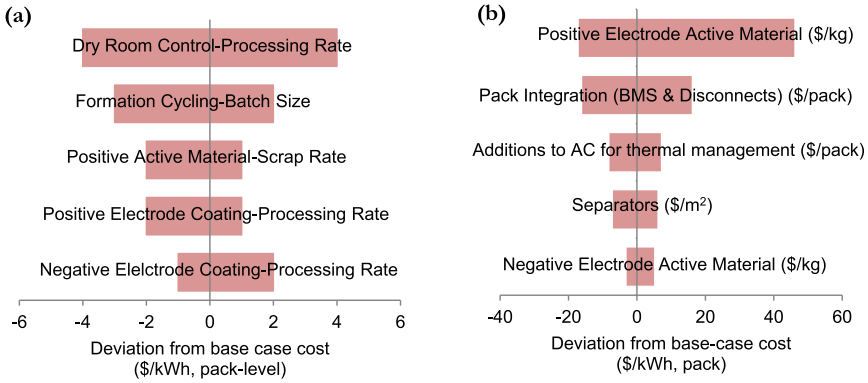

Fig. 10. Tornado plot showing the most sensitive (a) process step parameters and (b) material prices.

Table 7
Values considered for the sensitivity analysis of process step and material price parameters. The five most-sensitive process step and material price parameters have been reported.

		Units	Base value	Lower bound	Upper bound	Notes
Process step parameters	Dry-room control (air locks): processing rate	$m^2\ m^{-2}$ dry room area	0.03	−25%	+25%	Base value from ANL's BatPaC: 100 m^2 for an operating areas of 3000 m^2
	Formation cycling: batch size	cells $cycler^{-1}$	500	−25%	+25%	Base value from ANL's BatPaC Each equipment costs about $850 K
	Positive active material-scrap rate	%	9.8	−25%	+25%	Base value from ANL's BatPaC
	Positive electrode coating: processing rate	m min^{-1}	10	−25%	+25%	Base value from ANL's BatPaC
	Negative electrode coating: processing rate	m min^{-1}	10	−25%	+25%	Base value from ANL's BatPaC
Material prices	Positive electrode active material (NMC333)	\$ kg^{-1}	31	−25%	53	Base and upper bound value from ANL's BatPaC
	Pack integration (BMS and disconnects)	(\$ $pack^{-1}$)	435	−25%	+25%	Base value from ANL's BatPaC
	Additions to AC for thermal management	(\$ $pack^{-1}$)	200	−25%	+25%	Base value from ANL's BatPaC
	Separators	\$ m^{-2}	2	1	2.9	From ANL's BatPaC
	Negative electrode active material (graphite)	\$ kg^{-1}	19	17	23	From ANL's BatPaC

with plausible changes in positive electrode active material cost affecting pack-level cost by up to \$40 kWh^{-1}or more.

3.2. Optimal cell and pack designs

Table 8 summarizes optimal cell and pack designs, with their resulting cost, for each vehicle design (using energy and power requirements from Table 2).

The specific cost of the optimal design decreases with the vehicle's AER from \$545 kWh^{-1} for the $PHEV_{10}$ (16 km AER) to \$230 kWh^{-1} for the BEV_{200} (320 km AER). Part of this cost decrease is a result of increased cathode thickness for larger AER applications that have lower power requirements per unit energy. However, the $PHEV_{30}$ ($PHEV_{48}$ in kms) design is constrained by the upper bound for cathode thickness, and larger packs cannot take advantage of thicker electrodes. The additional reductions in specific cost observed for the $PHEV_{60}$ (96 km AER) and BEV_{200} (320 km AER) applications stem primarily from spreading some of the packaging, battery management and thermal control costs over a larger pack energy. In general, results suggest that the lowest cost designs use the thickest electrode coatings that satisfy the power requirements and large cell capacity and a preference for more cells per module instead of more modules per pack (because additional modules incur more module regulation costs, primarily from the module state-of-charge regulators). There is a marginal cost difference between achieving an active material target via increasing cathode thickness vs. increasing the number of bi-cell layers.

Fig. 11 shows a slice through the design space at the optimal point for the $PHEV_{10}$ (16 km AER) in Table 8 along the dimensions of cathode thickness (x^T) and bi-cell layers (x^L) (other variables fixed at $x^W = 99.5$ mm, $x^N = 6$, and $x^M = 4$). The cost minimizing solution is at the intersection of the energy constraint and the power constraint.

Fig. 12 shows that pack-level specific cost (\$ kWh^{-1}) for these designs varies almost linearly with power-to-energy ratio. In our base case, pack-level specific cost $\approx 27.129 r_{PE} + 191.2$ with $R^2 = 0.999$, where r_{PE} is the power to energy ratio. Fig. 12 also compares this result with predictions by Kromer and Heywood [25], who estimate battery costs by multiplying a base cost estimate for a high energy (48 kWh, BEV_{200}) pack C_B by a scaling factor that is a function of the power-to-energy ratio: $C = C_B f(r_{PE})$. They assumed C_B = \$300 kWh^{-1}, $f(r_{PE}) \in [4.5,5]$ in 2008, C_B = \$250 kWh^{-1},

Table 8
Optimization results for the base case. Boundary values are indicated with an asterisk. Vehicle all-electric-range (AER) shown in miles.

Vehicle	Cathode thickness (μm)	Cathode width (mm)	Num. bi-cell layers	Cells per module	Modules per pack	Cell capacity (Ah)	Pack cost (\$ $pack^{-1}$)	Specific cost (\$ kWh^{-1})
$PHEV_{10}$	65.3	75	51	6	4*	38.2	\$1970	\$545
$PHEV_{30}$	125*	100.5	22	9	4*	56.6	\$2615	\$325
$PHEV_{60}$	125*	99.3	22	19	4*	55.3	\$4380	\$265
BEV_{200}	125*	126	14	36	6	56.7	\$10,935	\$230

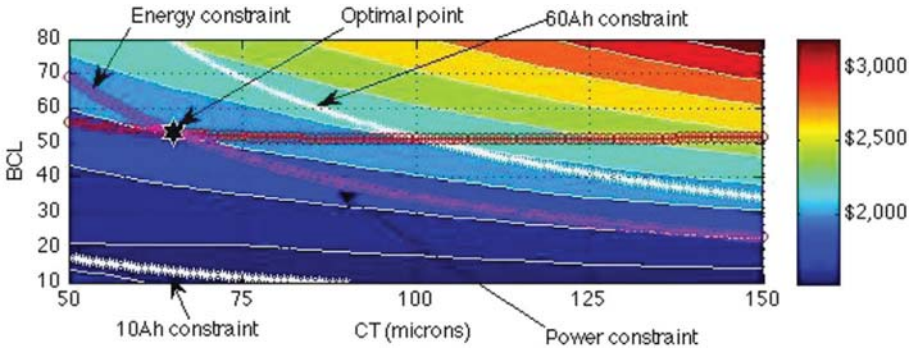

Fig. 11. Contour plot of cost as a function of the cathode coating thickness (x^T) and the number of bicell-layers (x^L) for the optimal $PHEV_{10}$ (16 km AER) design.

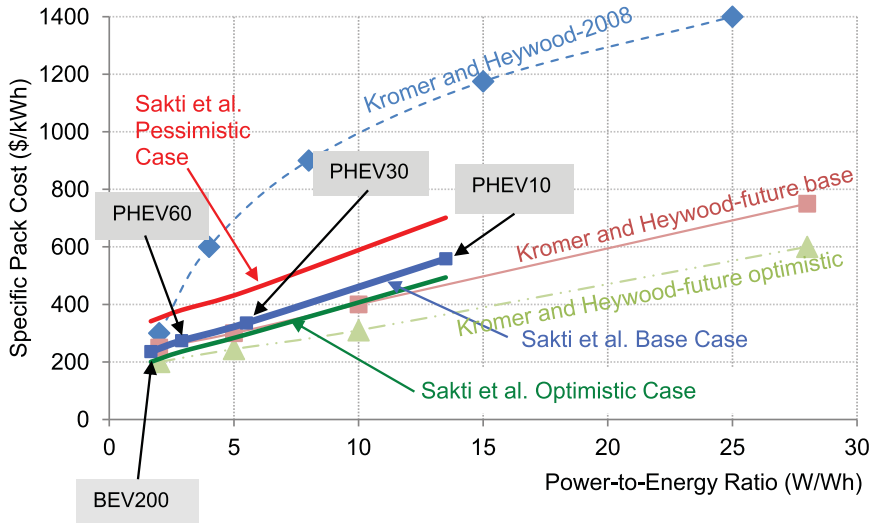

Fig. 12. Results from the cost and optimization model of this study using Kromer and Heywood's energy and power requirements for different vehicles with Kromer and Heywood predictions, 2008 [25], reproduced with permission from Matt Kromer. Vehicle all-electric-range (AER) shown in miles.

$f(r_{PE}) = 3$ for the future base case, and $C_B = \$200\ kWh^{-1}$, $f(r_{PE}) = 3$ for the future optimistic case. Our optimistic results are comparable to Kromer and Heywood's future base case.

Fig. 1 shows our base case cost estimates along with error bars representing our optimistic and pessimistic cost estimates compared to other cost estimates in the literature. Our estimates are generally in a similar range to others in the literature for the same time period, though some estimate that PHEV and BEV batteries will remain more expensive through 2020 or later. The figure also emphasizes the importance of vehicle application (especially AER) in determining cost, due in part to electrode thickness. Expert interviews as well as cell dissection suggest that manufacturers typically use thicknesses of about 75 μm on each side of the collector and are trying to achieve 125 μm. In our base case, the optimal cathode coating thickness for a $PHEV_{10}$ (16 km AER) is about 65 μm, and our estimated costs are similar to NAS/NRC estimates of 2012 Nissan Leaf (BEV_{73}: 117 km AER) and a Chevy Volt ($PHEV_{38}$: 61 km AER) battery costs [15]. Because we allow thicker electrodes (up to 120 μm in our base case), our larger packs have lower specific cost.

3.3. Sensitivity analysis

Fig. 13 summarizes optimal cathode coating thicknesses for $PHEV_{10}$ (16 km AER), $PHEV_{30}$ (48 km AER), $PHEV_{60}$ (96 km AER), and BEV_{200} (320 km AER) designs using different assumed values for maximum allowable cathode coating thickness: under pessimistic assumptions the thickness is capped at 100 μm; the base case cap is 125 μm; the optimistic cap is 200 μm; and the varying yield case has no active cap but assumes that thicker electrodes have lower yield. While battery design for $PHEV_{10}$ (16 km AER) requirements is not constrained by any of these thickness caps,

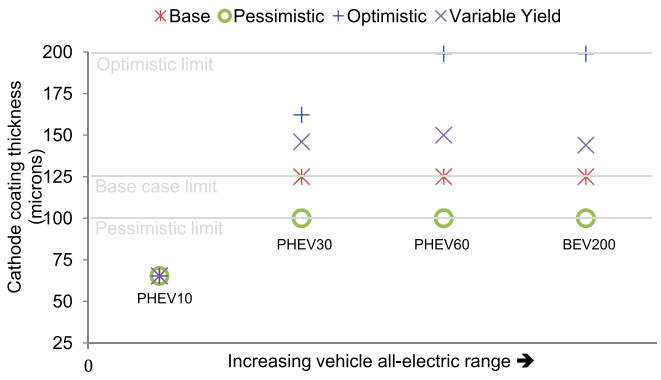

Fig. 13. Optimal cathode coating thickness for four scenarios. Vehicle all-electric-range (AER) shown in miles.

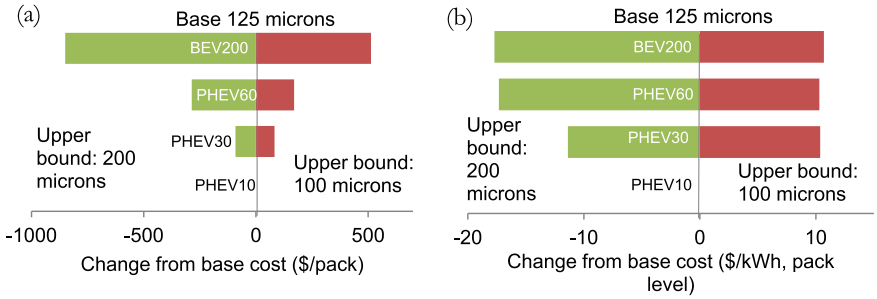

Fig. 14. Variation in battery pack (a) total cost and (b) specific cost due to variation in maximum allowable electrode coating thickness (base level = 125 μm, all other parameters from base case). Vehicle all-electric-range (AER) shown in miles.

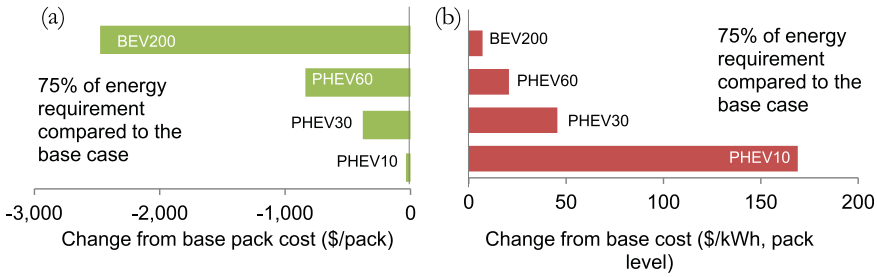

Fig. 15. Variation in battery pack (a) total cost and (b) specific cost due to a relaxed energy requirement (75% of base case, all other parameters from base case). Vehicle all-electric-range (AER) shown in miles.

increasing the maximum allowable thickness allows the larger battery packs to increase cathode thickness in order to reduce cost.

Figs. 14–16 summarize sensitivity of optimal pack cost to maximum allowable electrode coating thickness, pack energy requirements, and pack power requirements, respectively. Increasing the upper limit of the cathode coating thickness to 200 μm reduces cost of the BEV_{200} (320 km AER) pack by 8% ($850 or $18 kWh^{-1}) but does not reduce the cost of the $PHEV_{10}$ (16 km AER) pack. Relaxing the energy requirement by 25% (e.g.: due to increased efficiency) reduces BEV_{200} (320 km AER) pack cost by up to $2500 (specific cost increases slightly), and the $PHEV_{10}$ (16 km AER) specific cost increases dramatically (due to higher power to energy ratio) but still results in lower overall cost (due to lower capacity). Relaxing the power requirement by 25% (e.g.: due to lightweighting or blended operation) reduces pack cost by up to $90 ($16 kWh^{-1}) for a $PHEV_{10}$ (16 km AER) pack but generates no savings for the $PHEV_{30}$ (48 km AER), $PHEV_{60}$ (96 km AER), and BEV_{200} (320 km AER) whose power constraints are inactive.

Fig. 17 summarizes specific cost for each vehicle design, showing the base case, the variable yield case, and error bars representing the optimistic and pessimistic cases. Specific costs are pessimistically as high as $680 kWh^{-1} for the $PHEV_{10}$ reducing to $330 kWh^{-1} for a BEV_{200} (320 km AER) or optimistically as high as $480 kWh^{-1} for the $PHEV_{10}$ (16 km AER) reducing to $190 kWh^{-1} for the BEV_{200} (320 km AER). Overall, the effect of pack size on specific cost is larger than the uncertainty represented by our optimistic and pessimistic cases.

4. Summary and conclusions

We construct an optimization model to identify cost-minimizing NMC-G battery cell and pack designs as a function of cathode thickness, cathode width, and the number of bi-cell layers, cells per module, and modules per pack subject to energy, power, and capacity constraints.

With our cost model, derived partially from Argonne National Lab's BatPaC and modified to represent a process-based cost model, we find that economies of scale are achieved at relatively low production volume: around 30,000 packs per year in our base case for a 6.8 kWh pack. Our battery performance model, based on validated BDS simulations, models the effect of electrode thickness on battery power-to-energy ratio capabilities.

Assuming a base case production volume of 20,000 packs per year and power and energy requirements representative of $PHEV_{10}$ (16 km AER), $PHEV_{30}$ (48 km AER), $PHEV_{60}$ (96 km AER), and BEV_{200} (320 km AER) passenger vehicles, we optimize battery pack designs

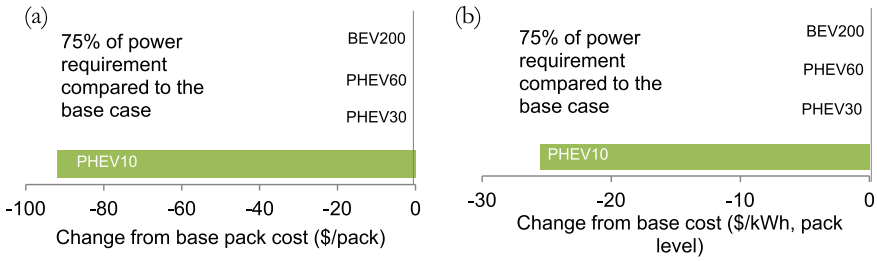

Fig. 16. Variation in battery pack (a) total cost and (b) specific cost due to a relaxed power requirement (75% of base case, all other parameters from base case). Vehicle all-electric-range (AER) shown in miles.

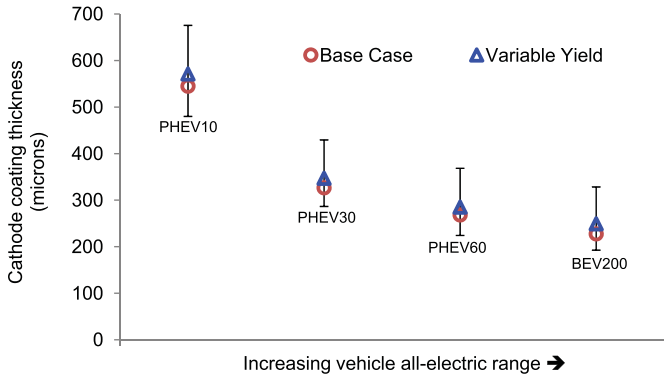

Fig. 17. Optimal pack level specific cost for each vehicle in base case and variable yield scenarios. Error bars represent optimistic and pessimistic scenarios. Vehicle all-electric-range (AER) shown in miles.

under base case, optimistic, and pessimistic scenarios as well as a scenario where yield varies with battery design. We find that optimal designs use high capacity cells and thicker electrodes for larger packs (which have lower power-to-energy requirements). Optimal specific cost increases almost linearly with the required power-to-energy ratio, and the effect is significant: switching from $PHEV_{10}$ (16 km AER) requirements to BEV_{200} (320 km AER) requirements reduces specific costs by 57% in our base case – a larger effect than the uncertainty represented by our optimistic and pessimistic scenarios. The reduced specific cost for larger packs is due to the ability to use thicker electrodes for applications with larger energy requirements (larger AER), and new technology enabling cathode thickness values up to 200 μm could further decrease costs of larger packs by up to 8%.

The significant variation of battery pack specific cost with pack size implies that prior studies comparing vehicles of differing AER that assume constant cost per kWh for all batteries may have unrealistic cost comparisons and should be reviewed and interpreted with care (e.g.: Refs. [3,5,8–12,46]).

4.1. Policy implications

The US federal government incentivizes plug-in vehicle sales via policy including the American Recovery and Reinvestment Act (ARRA) of 2009, which provides rebates for individuals who purchase certain PHEVs or BEVs [47]. If economies of scale in battery production are achieved at relatively low volume, as our process-based cost model suggests, then policies attempting to achieve reduced EV costs via subsidies for EV sales may have limited effects on battery costs beyond levels of ~200–300 MWh per year (approximate total sales of both the Chevy Volt and the Nissan Leaf through 2013 were about 23,000 vehicles each [48] or a total of about 900 MWh). Some additional cost reductions from increased sales due to learning, experience, and innovation are possible, but volume-based cost reductions appear to run out relatively quickly.

Additionally, our results emphasize that different cell and pack designs are appropriate for different applications. Customizing battery designs for each application may save costs (assuming adequate production volume), and policymakers should be careful not to assume that achievement of cost targets for one application necessarily enables cost targets to be achieved for other applications. Further, any cost estimate for automotive Li-ion batteries should be viewed in the context of the application (AER), the scope (cell vs. pack level costs), and the unit (cost per nameplate capacity vs. cost per usable capacity). Comparing cost estimates may be misleading if differences in context are not accounted for. However, significant uncertainty remains even when estimates are normalized by context.

4.2. Limitations

We study only the NMC-G Li-ion battery chemistry and do not consider alternative chemistries. NMC-G is a relevant and popular chemistry for automotive applications that is used either solely or in combination with other active material chemistries in the Ford C-Max Energi, BMW ActiveE, BMW I3, BMW I8, Mitsubishi I, Volvo C30 EV, Honda Fit EV and Honda Accord (personal comm. Ford & [49]). Other Li-ion chemistries, such as $LiFePO_4$ or $LiMnO_2$, are also relevant to vehicle design, and alternative chemistries beyond Li-ion are possible [49]. Our model assumes that cells in the battery pack are arranged in series, and we ignore vehicle system voltage requirements, though we do not expect this to affect our results significantly. We also ignore the potential effect of cell design on degradation characteristics and implications for life cycle cost or thermal management design. Lacking data on the effect of cell design on yield rates, we rely on expert judgment and assumptions for maximum allowable cathode thickness, and we similarly rely on expert judgment to estimate parameters in our process-based cost model. We assume that 10-s power tests are sufficient to determine a battery pack's power capabilities relative to vehicle peak power requirements. We intend that the model presented here be made publicly available for download and potential modification as new data become available.

Acknowledgments

The authors would like to thank Kevin Gallagher for his help with BatPaC, Robert Spotnitz for his help with Battery Design Studio®, and Orkun Karabasoglu for his help with Powertrain Systems Analysis Toolkit. Funding for this work came from a grant from the Gordon and Betty Moore Foundation, a grant from the National Science Foundation (CAREER grant #0747911), a grant from Toyota Motor Corporation, and a grant from the Research for Advanced Manufacturing in Pennsylvania (RAMP) program at Carnegie Mellon University. The findings and views expressed are those of the authors and not necessarily those of the sponsors.

Appendix A. Supplementary data

Supplementary data related to this article can be found at http://dx.doi.org/10.1016/j.jpowsour.2014.09.078.

References

[1] USEIA, Use of Gasoline, 2012. http://www.eia.gov/energyexplained/index.cfm?page=gasoline_use (accessed 09.09.13).
[2] L. Sanna, EPRI J. (2005). http://mydocs.epri.com/docs/CorporateDocuments/EPRI_Journal/2005-Fall/1012885_PHEV.pdf (accessed 27.12.10).
[3] C. Samaras, K. Meisterling, Environ. Sci. Technol. 42 (9) (2008) 3170–3176.
[4] J.J. Michalek, M. Chester, P. Jaramillo, C. Samaras, C.-S.N. Shiau, L.B. Lave, Proc. Natl. Acad. Sci. U. S. A. 108 (40) (2011) 16554–16558.
[5] C.-S.N. Shiau, S.B. Peterson, J.J. Michalek, in: ASME 2010 International Design Engineering Technical Conferences, 2010. DETC2010-28198.
[6] D.M. Lemoine, D.M. Kammen, A.E. Farrell, Environ. Res. Lett. 3 (2008) 014003.
[7] S. Plotkin, M. Singh, Multi-path Transportation Futures Study: Vehicle Characterization and Scenario Analyses, Argonne National Laboratory, 2009. Report No. ANL/ESD/09-5.
[8] D.M. Kammen, S.M. Arons, D.M. Lemoine, H. Hummel, in: D.B. Sandalow (Ed.), Plug-in Electric Vehicles – What Role for Washington?, Brookings Institution, Washington D.C., 2009.
[9] C.S.N. Shiau, C. Samaras, R. Hauffe, J.J. Michalek, Energy Policy 37 (2009) 2653–2663.
[10] J. Neubauer, A. Pesaran, J. Power Sources 196 (2011) 10351–10358.
[11] J. Neubauer, A. Brooker, E. Wood, J. Power Sources 209 (2012) 269–277.
[12] J. Neubauer, A. Brooker, E. Wood, J. Power Sources 236 (2013) 357–364.

[13] P. Albertus, J. Couts, V. Srinivasan, J. Newman, J. Power Sources 183 (2008) 771–782.
[14] J.F. Whitacre, The Economics and Science of Materials for Lithium Ion Batteries and PEM Fuel Cells, Working paper, Carnegie Mellon University, Pittsburgh, PA, 2009.
[15] National Research Council, Transitions to Alternative Vehicles and Fuels, The National Academies Press, Washington, D.C., 2013.
[16] R. Hensley, J. Newman, M. Rogers, Battery Technology Charges Ahead, McKinsey Quarterly, 2012.
[17] Boston Consulting Group, Batteries for Electric Cars: Challenges, Opportunities, and the Outlook to 2020, 2010. http://www.bcg.com/documents/file36615.pdf (accessed 27.07.10).
[18] National Research Council, Transitions to Alternative Transportation Technologies: Plug-in Hybrid Electric Vehicles, The National Academies Press, Washington, D.C., 2010.
[19] B. Barnett, J. Rempel, D. Ofer, B. Oh, S. Sriramulu, J. Sinha, M. Hastbacka, C. McCoy, PHEV Battery Cost Assessment (Slides), TIAX LLC, 2009.
[20] D.J. Santini, K.G. Gallagher, P.A. Nelson, Modeling of Manufacturing Costs of Lithium-ion Batteries for HEVs, PHEVs, and EVs, EVS-25, Shenzhen, China, 2010.
[21] E. Baker, H. Chon, J. Keisler, Technol. Forecast. Soc. Change 77 (2010) 1139–1146.
[22] M. Anderman, Feedback on ARB's Zero-emission Vehicle Staff Technical Report of 11/25/2009 Including Attachment A: Status of EV Technology Commercialization, 2010 (accessed 14.12.13), http://www.arb.ca.gov/msprog/zevprog/2009zevreview/anderman_review.pdf.
[23] California Air Resources Board, State of Preliminary Assessment of the Need for Revisions to the Zero Emission Vehicle Regulation, Attachment A: Status of ZEV Technology Commercialization, Technical Support Document, 2009.
[24] Frost & Sullivan, World Hybrid Electric and Electric Vehicle Lithium-ion Battery Market, N6BF-27, 2009.
[25] M.A. Kromer, J.B. Heywood, SAE Int. J. Engines 1 (1) (2008) 372–391.
[26] D.T. Ton, C.J. Hanley, G.H. Peek, J.D. Boyes, Solar Energy Grid Integration Systems Energy Storage, Sandia Report SAND2008-4247, 2008.
[27] F.R. Kalhammer, M.K. Kopf, D.H. Swan, V.P. Roan, M.P. Walsh, Status and Prospects for Zero Emissions Vehicle Technology, Report of the ARB Independent Expert Panel, Prepared for State of California Air Resources Board, 2007.
[28] A.A. Pesaran, T. Markel, H.S. Tataria, D. Howell, in: 23rd International Electric Vehicle Symposium (EVS-23) Anaheim, California, 2007.
[29] White House Office of Management and Budget, Table 10.1-Gross Domestic Product and Deflators Used in the Historical Tables: 1940–2018, 2013. http://www.whitehouse.gov/omb/budget/historicals (accessed 10.12.13).
[30] M.A. Kromer, J.B. Heywood, Electric Powertrains: Opportunities and Challenges in the U.S. Light-duty Vehicle Fleet, Sloan Automotive Laboratory, 2007. Publication No. LFEE 2007-03 RP.
[31] P.A. Nelson, K.G. Gallagher, I. Bloom, D.W. Dees, Modeling the Performance and Cost of Lithium-ion Batteries for Electric-drive Vehicles, Argonne National Laboratory, 2011.
[32] A. Sakti, J.J. Michalek, S.-E. Chun, J.F. Whitacre, Int. J. Energy Res. 37 (12) (2013) 1562–1568.
[33] USCAR, US DoE VTP Battery Test Manual for Plug-in Hybrid Vehicles, Rev 2, 2010. http://www.uscar.org/guest/article_view.php?articles_id=86 (accessed 11.02.13).
[34] Eureqa Formulize, User Guide and Resources, 2014. http://nutonian.wikidot.com (accessed 05.03.14).
[35] G.G. Gallagher, P.A. Nelson, D.W. Dees, J. Power Sources 196 (2011) 2289–2297.
[36] Y. Asiedu, P. Gu, Int. J. Prod. Res. 36 (4) (1998) 883–908.
[37] I.F. Weustink, E. Ten Brinke, A.H. Streppel, H.J.J. Kals, J. Mater. Process. Technol. 103 (1) (2000) 141–148.
[38] N.S. Ong, Int. J. Prod. Econ. 38 (2–3) (1995) 159–172.
[39] J. LaTrobe-Bateman, D. Wild, Res. Eng. Des. 14 (2003) 107–117.
[40] J.V. Busch, F.R. Field III, in: D. Rosato, D. Rosato (Eds.), The Blow-molding Handbook, Hansr Publishers, New York, 1998.
[41] R. Kirchain, F. Field, Process-based Cost Modeling: Understanding the Economics of Technical Decisions, Encyclopedia of Materials Science and Engineering, 2000.
[42] E. Fuchs, E. Bruce, R. Ram, R. Kirchain, J. Lightwave Technol. 24 (8) (2006) 3175–3186.
[43] E. Fuchs, F. Field, R. Roth, R. Kirchain, Compos. Sci. Technol. 68 (9) (2008) 1989–2002.
[44] K. Kuipers, BNB20, 2000. http://www.mathworks.com/matlabcentral/fileexchange/95-bnb (accessed 06.03.14).
[45] R. Brodd, Battery/Cell Manufacturing Cost Study, in: International Meeting on Li-ion Batteries, 2010.
[46] S.B. Peterson, J.F. Whitacre, J. Apt, J. Power Sources 195 (8) (2010) 2377–2384.
[47] Internal Revenue Services, Energy Incentives for Individuals in the American Recovery and Reinvestment Act, US Gov., 2010. http://www.irs.gov/newsroom/article/0,,id=206875,00.html (accessed 12.10.10).
[48] Z. Shahan, Chevy Colt Sales Inch Out Nissan Leaf Sales in 2013, Clean Technica, 2014. http://cleantechnica.com/2014/01/05/chevy-volt-sales-inch-nissan-leaf-sales-2013/ (accessed 25.03.14).
[49] The National Petroleum Council, Advancing Technology for America's Future, 2012. http://www.npc.org (accessed 25.03.14).